

Time and space resolved current density mapping in three dimensions using magnetic field probe array in a high voltage coaxial gap

S. W. Cordaro, and S. C. Bott-Suzuki

Citation: *Journal of Applied Physics* **122**, 213303 (2017);

View online: <https://doi.org/10.1063/1.5002698>

View Table of Contents: <http://aip.scitation.org/toc/jap/122/21>

Published by the *American Institute of Physics*

Articles you may be interested in

[Plasmonic and metallic optical properties of Au/SiO₂ metal-insulator films](#)

Journal of Applied Physics **122**, 213101 (2017); 10.1063/1.5003302

[High-intensity discharge lamp and Duffing oscillator—Similarities and differences](#)

Journal of Applied Physics **122**, 213302 (2017); 10.1063/1.4999979

[Dynamic analysis of reactive oxygen nitrogen species in plasma-activated culture medium by UV absorption spectroscopy](#)

Journal of Applied Physics **122**, 213301 (2017); 10.1063/1.4999256

[Manipulating broadband polarization conversion in metamaterials](#)

Journal of Applied Physics **122**, 215101 (2017); 10.1063/1.4997972

[One-way transmission of electrons on the topological insulator surface modulated by magnetic potential](#)

Journal of Applied Physics **122**, 214301 (2017); 10.1063/1.5002728

[Perspective: Terahertz science and technology](#)

Journal of Applied Physics **122**, 230901 (2017); 10.1063/1.5007683



Scilight

Sharp, quick summaries **illuminating**
the latest physics research

Sign up for **FREE!**

AIP
Publishing

Time and space resolved current density mapping in three dimensions using magnetic field probe array in a high voltage coaxial gap

S. W. Cordaro^{a)} and S. C. Bott-Suzuki

Center for Energy Research, University of California San Diego, La Jolla, California 92093, USA

(Received 31 August 2017; accepted 19 November 2017; published online 7 December 2017)

We present an experimental analysis of the symmetry of current density in a coaxial geometry, diagnosed using a magnetic field probe array and calculations of the Fowler-Nordheim enhancement factor. Data were collected on the coaxial gap breakdown device (240 A, 25 kV, 150 ns, ~ 0.1 Hz), and data from experiments using 2 different gap sizes and different penetration depths are compared over runs comprising 50 shots for each case. The magnetic field probe array quantifies the distribution of current density at three axial locations, on either sides of a vacuum breakdown, and tracks the evolution with time and space. The results show asymmetries in current density, which can be influenced by changes in the gap size and the penetration depth (of the center electrode into the outer electrode). For smaller gap sizes (400 μm), symmetric current profiles were not observed, and the change in the penetration depth changes both the symmetric behavior of the current density and the enhancement factor. For larger gaps (900 μm), current densities were typically more uniform and less influenced by the penetration depth, which is reflected in the enhancement factor values. It is possible that the change in inductance caused by the localization of current densities plays a role in the observed behavior. *Published by AIP Publishing.*

<https://doi.org/10.1063/1.5002698>

INTRODUCTION

Vacuum gap breakdown at high voltages, typically in the range of tens of kilovolts to megavolts, occurs in many systems, particularly where high current conduction is required. Several standard geometries, such as sphere-sphere, plane-plane, and point-plane, have been extensively investigated under both pulsed and D.C. conditions and, in general, are well understood and documented.¹⁻⁵ To date, no detailed analysis of coaxial geometry has been performed. This is despite this geometry being a common feature of high energy devices including in vacuum transmission lines and switch systems.

The present work is motivated by the need to better understand the mechanisms by which breakdown initiation occurs in a coaxial gap over a few nanoseconds to a few microseconds at tens of kV at gap sizes of up to 1 mm. Of specific interest is the evolution of the magnetic field in time and space along the gap and how any asymmetries about the azimuth of this gap influence this evolution. Any asymmetry in breakdown about the azimuth could be responsible for non-uniform distributions of voltage and current which could lead to early time scale instabilities of a load at the termination of a transmission line. A particular case of significant interest at present is the MagLIF⁶ design on Sandia's Z-machine, where one mounting system maintains a coaxial vacuum gap in the power feed as the machine voltage is applied. Often, in such large devices, a direct observation of vacuum gaps is not feasible, and a comprehensive method to observe and (potentially) influence the evolution of the magnetic field and current density would prove beneficial. Here, we used an extensive array of magnetic field probes to

examine the current density uniformity along a coaxial geometry under pulsed current conditions.

EXPERIMENTAL DESIGN AND ANALYSIS METHODS

An experimental system was previously developed to study the mechanisms and influences of coaxial geometry vacuum gaps.⁷ This table top experiment was performed on a Coaxial Gap Breakdown (CGB) machine; it consists of two aluminium electrodes, a hollow cylinder with an inserted solid cylinder, both of which are attached to electrical 3-D translational mounts so as to ensure the electrodes are parallel to one another and to control their relative positions (Fig. 1). Electrodes can be readily machined to create any azimuthal gap required in the coaxial geometry, 25 μm to several millimeters. In this initial study, we examine 2 azimuthal gap sizes, 400 μm and 900 μm , and penetration depths (PDs) of the central conductor into the hollow (outer) electrode from 3.72 mm to 9.88 mm. It is important to note that while the



FIG. 1. Coaxial gap experiment with b-dot array zones labeled.

^{a)}scordaro@ucsd.edu. URL: www.p3ucd.com.

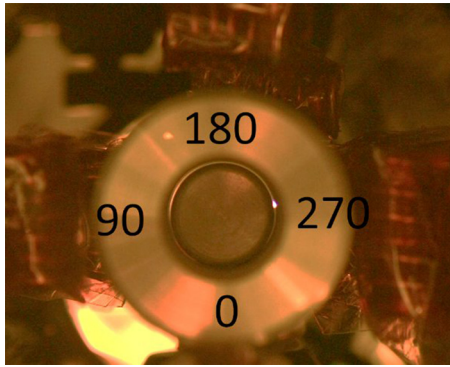


FIG. 2. Time-integrated optical image of vacuum gap breakdown for a 400 μm gap, showing the location of the breakdown at $\sim 270^\circ$.

electrodes used for this work are cleaned following machining, they are not further polished or treated.

Experiments were performed under vacuum ($<10^5$ Torr) and at room temperature. A high voltage pulse (25 kV, 150 ns, Fig. 7) is delivered via a charge circuit to the coaxial gap driving ~ 240 A through the gap. The device is repetition rated at ~ 0.1 Hz, and this allows for statistical analysis to be performed, with examination of each gap size of penetration depth comprising 50–1000 shots. The vacuum gap was monitored electrically by Pearson coil (model 6585, 1.5 ns rise time), and a pair of high voltage probes (Pintek-HVP-39pro) located at the high voltage and ground sides of the electrodes. Time-integrated optical images are taken along the electrode common axis for every shot, and the current density is monitored by an array of magnetic (dB/dt) probes⁸ as described below.

The methodology to determine the azimuthal symmetry of breakdown and how it influences the current density were described previously, using 3 probes located at different

azimuthal positions at the same axial point on the electrode system.⁷ The relative strengths of the magnetic field recorded by each of the probes is used to triangulate the average position of the current as a function of time. This proved highly successful, and the probe array was extended to include 2 additional axial positions, each with 3 probes to give a total of 9 probes reporting the azimuthal current density symmetry at 3 different axial positions.

The array geometry used here is given in Fig. 1. A set of 3 probes are spaced at 120° around the azimuth and separated by 30 mm along the axial direction. The exact location of each probe relative to the electrodes is recoded via the spatially calibrated optical images. The zones are labelled Zone 1 (close to the high voltage connection), Zone 2 (at the position of the coaxial vacuum gap) and Zone 3 (close to the ground connection).

Using a triangulation technique for each zone, we are able to map the evolution of the current density over the duration of the current pulse (150 ns) and as the pulse travels along the length of the electrodes (~ 92 mm). To illustrate this, we take the case where a breakdown occurs at the 270° position of a 400 μm gap. In Fig. 2, the time integrated optical images show the location of the breakdown for this shot, and Fig. 3 shows the raw magnetic field probe data for all probes along with the current trace. Note how the magnetic field probe signal generally follows the trend of the current, and is expected, but with different magnitudes observed between probes at different azimuthal locations.

Analysis of the probe data for each zone is carried out using an in-house data analysis program which uses the probe location and the measured field strength to construct a circle of a radius consistent with the total current recorded. A smaller circle for a given probe indicates that, on average, the current density is flowing closer to that probe than one

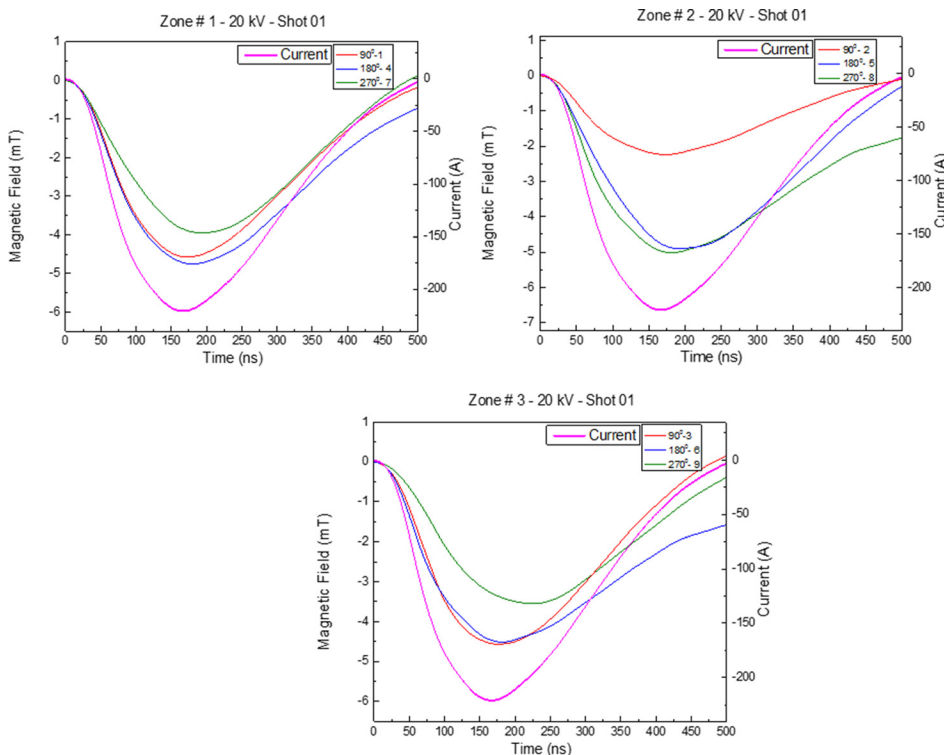


FIG. 3. Magnetic field traces, 400 μm gap, Al linear-breakdown at $\sim 270^\circ$.

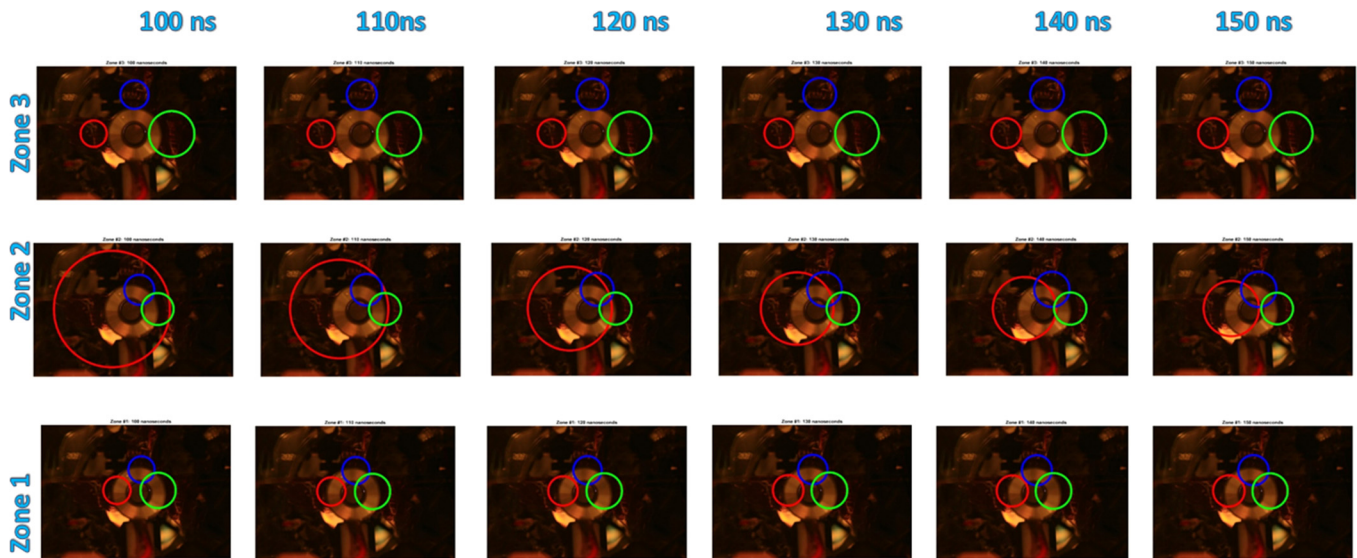


FIG. 4. Triangulation matrix, the color of each zone corresponds to the azimuthal position, as in Fig. 3. Red-90, Blue-180, Green-270.

with a larger calculated circle radius. In the ideal case, all probe circles overlap at a single position, as was observed in previous work.⁷ The plots on which the circles are overlaid on the probe position are referred to as triangulation plots.

To simplify the analysis for all three zones, triangulation plots are calculated every 10 ns during the current drive and compared to the optical image of the electrodes (Fig. 4).

The triangulation plots show distinct behaviors between each zone. In Zone 1, 100 ns, the magnetic field probes indicate the current density is in the 90–180 region, closer to the smaller red and blue circles and further from the larger green circle. In Zone 2, at the same time, the current density has shifted towards the breakdown position at ~270° (blue and green circles are small, and red ones are large). In Zone 3, the current density returns to the 90–180° region seen in zone 1. These distinct offsets remain constant throughout the 50 ns duration as seen in the matrix above. Where the three probes circles overlap at a single position, it is possible to exactly locate the current density. This can be seen, for example, in Zone 2 at 140 ns which corresponds to the optical image location of the breakdown. Often, only an approximate location is possible as outlined here. However, even

this highlights significant motion and non-uniformity for different electrode setups.

In order to better understand how the magnetic field evolves from shot-to-shot, a method was devised in which the coaxial gap time integrated image is broken into a standard quadrant system with Quadrant 1 always centered at the breakdown position (Fig. 5). This simplifies the discussion and highlights large motions of the average current density position throughout the current drive timescale.

Combining the quadrant system with the triangulation method yields a quadrant map of the magnetic field evolution, taken at 10 ns intervals during the current drive. Figure 5 shows the result of applying this methodology to a shot with a 400 μm gap and a 3.03 mm penetration depth of the cathode in the anode that has a breakdown around 90°. The resulting plot is given in Fig. 6.

Zone 2 is the simplest, since this is the location of the breakdown across the gap, and we define this region as Quadrant 1. We, therefore, see that Zone 2 stays at Quadrant 1

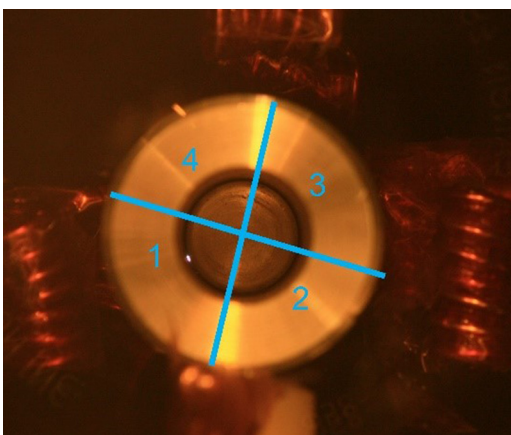


FIG. 5. Coaxial gap quadrant overlay; 400 μm, PD-3.03 mm, 25 kV.

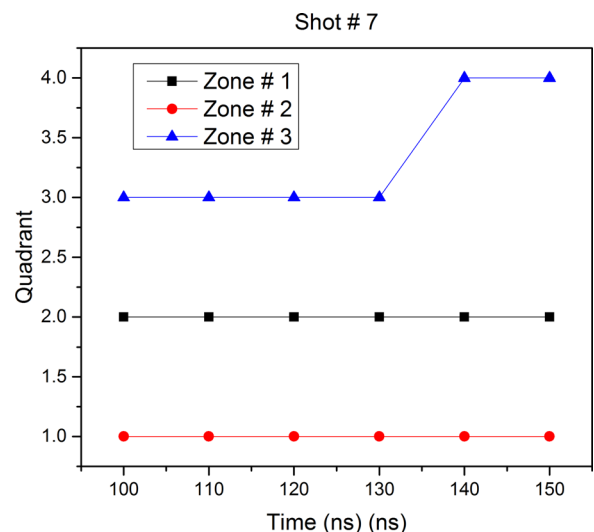


FIG. 6. Quadrant mapping, corresponding to Fig. 5.

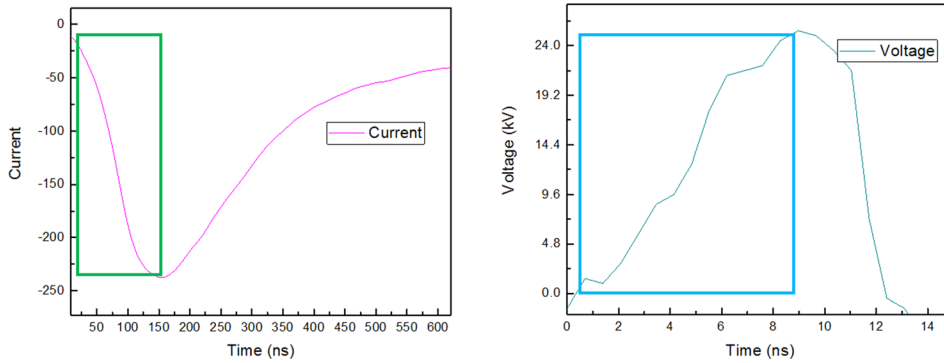


FIG. 7. Standard current and voltage signals, 400 μm , PD - 6.33 mm.

throughout the experiment. In Zone 1, the current density remains in Quadrant 2 from 100 ns to 150 ns. In Zone 3, a transition of the current density from quadrant 3 to quadrant 4 is observed between 130 ns and 140 ns. From this individual quadrant map plot, a persistent offset in current density is observed in the presence of an asymmetrical breakdown in the gap. The motion of the current density is observed, and the current density at locations up- and down-stream of the breakdown does not correspond to its azimuthal location.

In addition to the imaging analysis, the recovery of electrical data on every shot allowed the characterization of the breakdown process through calculation of the Fowler-Nordheim (FN) enhancement factor⁴ for each case. This describes the likely breakdown voltage of an electrode set over and above that, expected as a result of the material work function alone. As discussed above, the electrodes in this work are unpolished, and so we expect values of the enhancement factor to be relatively large. Following the procedures adopted by Okawa *et al.*,¹ measurements are taken of the rising edge of the voltage trace before breakdown, as seen in Fig. 7 outlined in blue, and the current rise to the peak, outlined in green.

These values for each shot are taken and plotted as I/V^2 against $1/V$. The resulting graph yields a line, and the slope of this line gives the enhancement factor, β , for that respective geometry. We can then directly examine how the FN enhancement factor changes for our 4 geometries. Figure 8 shows the FN plots for a gap size of 400 μm at penetration depths of 3.03 mm and 6.33 mm.

The evaluation of enhancement factors allows a comparison of the expected breakdown behaviors across different geometries.

RESULTS AND DISCUSSION

The quadrant mapping technique and the F-N analysis were applied to 50 shots in each of 4 geometries: a 400 μm gap with penetration depths of 3.03 mm and 6.33 mm and a 900 μm gap with penetration depths of 3.72 mm and 9.88 mm.

Figure 9 shows the variation in both the enhancement factor and the quadrant mapping resulting from the change in the penetration depth from 3.03 mm and 6.33 mm for a 400 μm gap. For smaller penetration depths, typical enhancement factors values are approximately -5 A/V with the larger depth being approximately -1.7 A/V . This is a difference of a factor of ~ 2.8 . The quadrant mapping method, which shows all 50 shots in this run, also shows a change between the two penetration depths. At PD = 3.03 mm, the current density can occupy any of the 4 quadrants in both Zones 1 and 3. There is also some limited motion between quadrants during the experiment. It is noticeable that the current density does not look uniform at any time for these shots. When the penetration distance is increased to PD = 6.33 mm, there is distinct difference in behavior. Most notably, transitions in Zone 3 and Zone 1 are constrained to quadrants 3 and 4 in Zone 3, and constrained to quadrants 3, 2 and 1 after 100 ns in Zone 1. Again, there is a persistent changing non-uniformity on either side of asymmetric azimuthal breakdowns over 50 shots and across the length of the electrodes and tens of nanoseconds.

The results of analysis for 900 μm gap shots are shown in Fig. 10. At penetration depths of 3.72 mm, the enhancement factor is $\sim -1.3 \text{ A/V}$, several times smaller than the factor for the 400 μm gap shots at similar depths. When the penetration depth is increased, however, the variation in

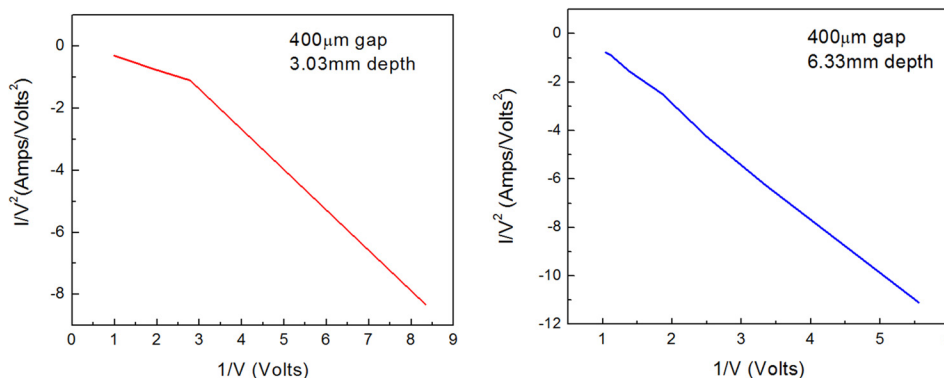


FIG. 8. Fowler-Nordheim plots for a 400 μm gap at penetration depths of 3.03 mm and 6.33 mm.

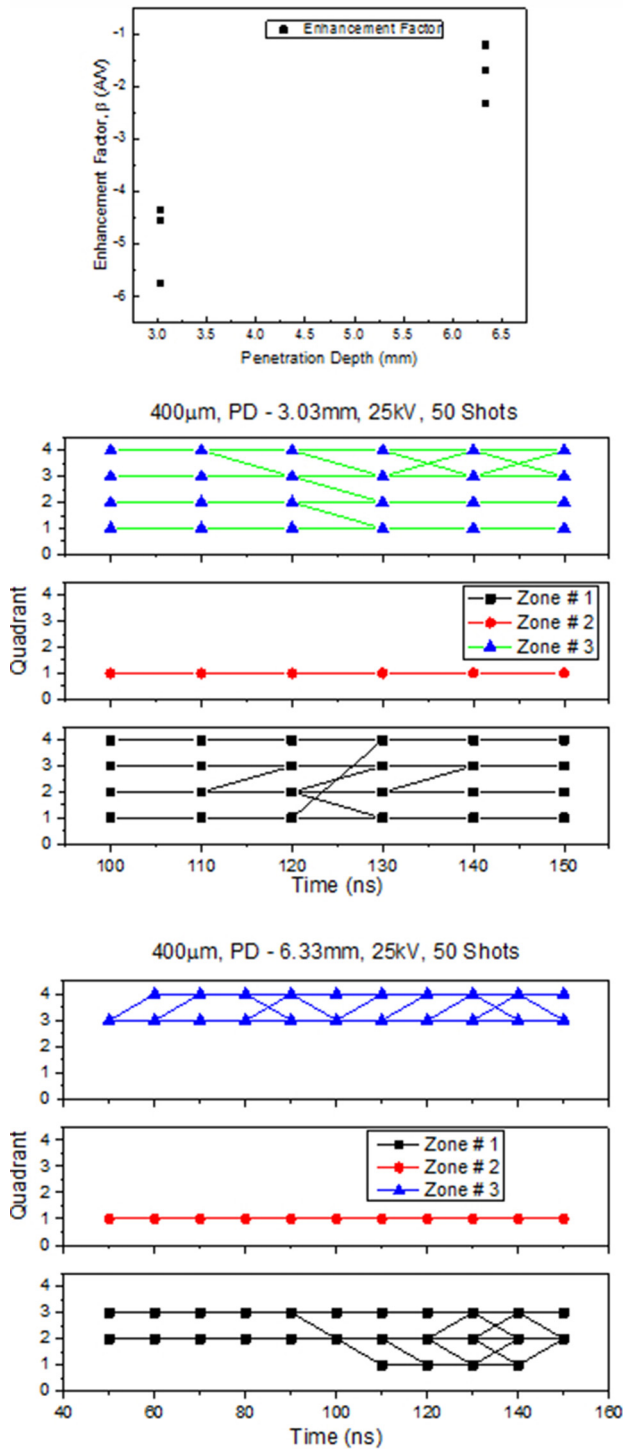


FIG. 9. FN enhancement factor and quadrant maps for 400 μm gaps at different penetration depths.

the enhancement factor is very small, with values of ~ -1.5 A/V. This is similar to the values of the larger penetration depth for smaller gaps.

The quadrant mapping shows several interesting features. Firstly, note that there are now vertical lines for all times examined in both Zones 1 and 3. This denotes that for many shots, the current density was uniformly distributed around the electrode; i.e., occupying all 4 quadrants at the same time. This was not seen for the smaller gap sizes. Additionally, there are more transition occurring, as the

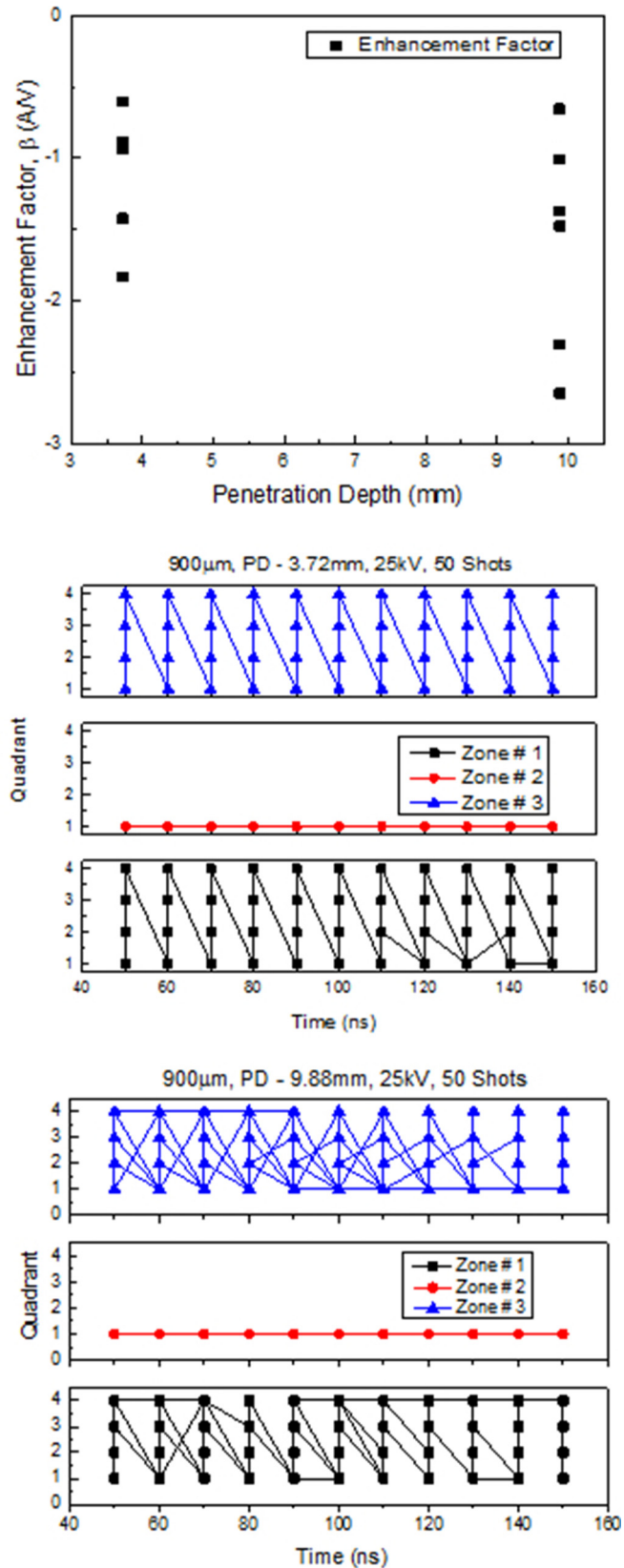


FIG. 10. FN enhancement factor and quadrant maps for 900 μm gaps at different penetration depths.

current density moves around the electrode. For smaller penetration depths, these almost entirely occur from Quadrant 4 to zone 1. It appears here that the current density is either uniform or offset close to the position of the breakdown in

Quadrant 1. For larger penetration depths, whilst uniform current density is also observed at all times, there is also significantly more motion of the current density between all quadrants. This suggests that the position of breakdown has less effect in influencing the offset of the current density.

It is possible that the FN enhancement factor is affected by the inductance change caused by the actual current density distribution at the electrodes. The skin depth at the electrode surface is of the order of $100\ \mu\text{m}$, and the quadrant mapping resulting from the magnetic field probe measurements denote the uniformity of this azimuth. For the $400\ \mu\text{m}$ gap experiments, the current is never observed to be uniform, and typically is observed in only one quadrant. For the $900\ \mu\text{m}$ case, uniformity is regularly observed, with some transitions to localized current density. If we take these two disparate cases, it is possible to suggest how the inductance is expected to change as the penetration depth changes.

Simplistically, in the case where the current occupies only 1 quadrant, we can treat it as a parallel wire case, wherein the current flows only in a circular cross-section determined by the skin depth of $100\ \mu\text{m}$ and the separation of the two “wires” is the gap size. All cases for the $400\ \mu\text{m}$ gap can be treated in this way, giving values of $\sim 2.5\ \text{nH}$ for the $3.03\ \text{mm}$ penetration depth, and $\sim 5\ \text{nH}$ for the $6.33\ \text{mm}$ depth. This is comparable to the other inductances in the circuit, and so may affect the calculation of the enhancement factor since this is calculated from the current and voltage traces.

In the uniform current density cases, we can calculate the inductance as a co-axial cable, and this applies to all the $900\ \mu\text{m}$ cases. Here, the changes caused by the penetration depth will still cause a linear change in the inductance, but the absolute values are smaller; $\sim 0.06\ \text{nH}$ for the $3.72\ \text{mm}$ case and $0.16\ \text{nH}$ for the $9.88\ \text{mm}$ case. These are significantly smaller than the circuit values, and are unlikely to affect the current drive indirectly. We, therefore, do not observe a change in the calculated enhancement factor with a change in the penetration depth. This analysis suggests that this case must be taken into account while carrying out estimations of the FN enhancement factors for coaxial geometries, since we directly measure significant current density asymmetries in many cases.

CONCLUSIONS

In this work, we have shown that asymmetries in the azimuthal breakdown position have an influence on the asymmetric current distribution in time and space. These

asymmetries in current density can be influenced by changes in the gap size and the penetration depth, and have been measured experimentally as a function of time and space with a newly developed diagnostic approach.

For experiments using a $400\ \mu\text{m}$ gap, as the penetration depth is increased to $6.33\ \text{mm}$, a distinct preference in the azimuthal location of the current density occurs that is not present in the $3.03\ \text{mm}$ penetration depth. A factor of ~ 3 change occurs in the enhancement factor at this gap size when the penetration depth is increased from $3.03\ \text{mm}$ to $6.33\ \text{mm}$. For the $900\ \mu\text{m}$ gap, we have shown that on either side of an azimuthal asymmetry in breakdown, symmetry and asymmetry can occur regularly. When the penetration depth is increased, a nominal change is seen in the enhancement factor, but quadrant mapping shows an increase in current density distribution transitions between quadrants, as well as slight asymmetries where the current density is distributed in three quadrants and can undergo transition between slight asymmetry to asymmetry and back again in ten nanoseconds.

Future studies will focus on extended parameter scans of the gap size and the penetration depth, electrode materials and surface preparation to determine the change in the FN enhancement factor in co-axial geometry for comparison with the literature.

ACKNOWLEDGMENTS

This work was supported under the NNSA SSAA program through DOE Cooperative Agreement No. DE-FC03-02NA00057.

¹M. Okawa, T. Shioiri, H. Okubo, and S. Yanabu, *IEEE Trans. Electr. Insul.* **23**(1), 77 (1988).

²G. P. Beukema, *Physica* **61**, 259–274 (1972).

³D. Nicolaescu, *J. Vac. Sci. Technol. B* **11**, 392 (1993).

⁴R. J. Harvey, R. A. Lee, A. J. Miller, and J. K. Wigmore, *IEEE Trans. Electron Devices* **38**, 2323–2328 (1991).

⁵R. H. Fowler and L. Nordheim, “Electron emission in intense electric fields,” *Proc. R. Soc.* **119**, 173–181 (1928).

⁶S. A. Slutz, M. C. Herrmann, R. A. Vesey, A. B. Sefkow, D. B. Sinars, D. C. Rovang, K. J. Peterson, and M. E. Cuneo, *Phys. Plasmas* **17**, 056303 (2010).

⁷S. W. Cordaro, S. C. Bott-Suzuki, L. S. Caballero Bendixsen, L. Atoyian, T. Byvank, W. Potter, B. R. Kusse, and J. B. Greenly, *Rev. Sci. Instrum.* **86**, 073503 (2015).

⁸J. B. Greenly, J. D. Douglass, D. A. Hammer, B. R. Kusse, S. C. Glidden, and H. D. Sanders, *Rev. Sci. Instrum.* **79**, 073501 (2008); J. Greenly, M. Martin, I. Blesener, D. Chalenski, P. Knapp, and R. McBride, *AIP Conf. Proc.* **1088**, 53 (2009).